Electrical Response of Silicon Heterojunction Solar Cells with Transparent Conductive Oxide Antireflective Coating

M. Perný[a], V. Šály[a], V. Ďurman[a], J. Packa[a], J. Kurcz[a], M. Mikolášek[b] and J. Huran[c]

[a] *Institute of Power and Applied Electrical Engineering, Slovak University of Technology, Ilkovičova 3, 812 19 Bratislava, Slovakia*
[b] *Institute of Electronics and Photonics, Slovak University of Technology, Ilkovičova 3, 812 19 Bratislava, Slovakia*
[c] *Institute of Electrical Engineering, Slovak Academy of Sciences, Dúbravská cesta 9, 841 04 Bratislava, Slovakia*

Received: 14.07.2020 & Accepted: 22.10.2020

Doi: 10.12693/APhysPolA.139.39 *e-mail: milan.perny@stuba.sk

This work is focused on the results of the development of solar photovoltaic heterostructures which consist of a combination of amorphous silicon carbide (used as emitter), doped crystalline silicon substrate and deposited thin transparent conductive oxide layer. Two types of transparent conductive oxide layers: indium tin oxide and indium zinc oxide were prepared for the investigation. The advantages and benefits of the conductive oxides applied on prepared solar cell structures are described in this paper. The main contribution of the work is the assessment of the impact of a sputtering current applied at transparent conductive oxide deposition on the resulting photovoltaic properties. It was found that all electrical (charge carrier mobility, electrical conductivity, photovoltaic parameters) as well as optical (transmittance) parameters are strongly dependent on the sputtering setup. The analyses were performed on both, prepared photovoltaic heterostructures and transparent conductive oxide layers deposited on the glass using DC and AC measurement and optical techniques. The sputtering conditions were optimized to get the best photovoltaic behaviour.

topics: heterojunction solar cell, ITO, IZO, amorphous silicon carbide

1. Introduction

Energy plays a key role in today's society. It is increasingly accepted that renewable energy should have an important place in the energy sector in future. Photovoltaics (PV) plays a considerable role in the renewable energy mix. Many photovoltaic materials and structures are currently already commercially available in PV modules [1]. The theoretical efficiency of homojunction solar cells according to the Shockley–Queisser calculation give a maximum value of 33.7% at 1.34 eV semiconductor, 38% for two junction structures (GaInP/GaAs/Ge) and 46% for multijunction structure under concentrated light. Practically/commercially available solar cells are gradually approaching these values. In the case of the actually developed solar cells, the efficiency obtained in laboratory conditions is, e.g., 13.5% for organic, 21.6% for perovskite, 12.7% for a-Si/nc-Si (tandem cell), 26.7% for crystalline silicon and 29.1% for a GaAs solar cell. The highest laboratory efficiency of 39.2% was achieved on the six-junction monolithic structure. The efficiency of the commercially available cells and modules is lower. The highest efficiency for a commercially available solar module is up to date 22.70% [2]. It is possible to increase these values, e.g., by multijunction approaches or other technological steps (such as, for example, reducing an absorption loss) [3].

A constant increase of the PV conversion efficiency of various material structures, while price and energy consumption during the production process should remain stable, is a constant challenge for researchers from the academic and industry sectors. One of acceptable solutions is the solar heterojunction photovoltaic technology (SHJ).

The SHJ technology combines several advantages such as a simple and low temperature preparation technology, e.g., in the case of deposition processes of amorphous silicon (a-Si:H) and its modification (also doped silicon carbide a-SiC:H) which allows the preparation of large-area structures. The technology is environmentally friendly and economically attractive. Finally, the cells are characterized with a higher value of open circuit voltage (above 700 mV) [4] and a considerably lower temperature coefficient than that of conventional silicon solar cells.

The SHJ concept is based on the combination of conventional photovoltaic material (crystalline silicon used as a substrate) while the junction is created by the deposition of p or n (depending on the substrate type) doped amorphous silicon or silicon carbide used as an emitter. Intrinsic a-Si:H layer is incorporated as a passivation layer. The back side is usually back surface field (BSF) adjusted but not used in our experiment. An equally important element of this structure is a passivating contact; in our study it is a thin conducting oxide film which also performs a function of a charge carrier collector from the entire solar cell area [5].

The potential of this technology can be clearly illustrated with the progress over the last 10 years. The fill factor was increased from 80% to 85% and the efficiency from 23% to 26.7% [6, 7]. Despite these promising outcomes, a number of other challenges remain for applied research including the development of configuration of a structure, e.g., two-side contacted SHJ solar cells, optimization of preparation of thin conducting charge collection layer, preparation of homogeneous amorphous layer, improvement of the interface between crystalline silicon and the amorphous layer, reduction of series resistance value, etc.

The role of a transparent conductive layer in the SHJ technology is twofold. In the case of a front junction (monofacial configuration), it serves as an effective collector of generated charges which results in higher short circuit current, lower value of series resistance, and higher quantum efficiency. At the same time, its function is also of an antireflective and passivation layer for amorphous silicon. Such a layer should also meet other requirements, e.g., the adequate refractive index and thickness. The availability of the low temperature deposition method (less than 200°C) is important to avoid the damage of the amorphous structure [8]. All these requirements including a suitable energy gap (> 3 eV) and transparency for visible light are fulfilled by transparent conducting oxide.

TCO are metal oxides. Indium tin oxide (ITO) is very commonly used. ITO can be tuned to increase its conductivity and improve solar cell performance [9]. Indium tin oxide, fluorine doped tin oxide (FTO), indium zinc oxide (IZO), Al-doped zinc oxide (AZO) and indium cadmium oxide are currently being researched and applied in thin-film photovoltaics. The mentioned transparent oxides are referred to either as doped oxides or alloys [10, 11]. Structures in the form of a polycrystalline or amorphous thin film used as a window layer can be prepared by various techniques, including RF or DC magnetron sputtering, chemical vapour deposition or pulsed laser deposition [12]. Commercial and academic research in this area is currently focused on further optimization of deposition techniques resulting in better electrical and optical properties of prepared layers.

The technology optimization can be illustrated in the process of layer preparation using RF deposition, where the optimal sputtering deposition parameters, such as the concentration of the gasses and power of the reactor, are being researched. Appropriate setting of the deposition parameters results in a higher short circuit current and fill factor of the obtained solar heterostructure.

The core of the present work is focused on the presentation of research results of the preparation of thin layers of conductive metal oxides and based on former experimental expertise already presented in [13]. The results of an optimization of the ITO and IZO deposition process for SHJ cells are shown here using electrical and optical techniques.

2. Experimental setup

The photovoltaic samples were heterostructures of p-type monocrystalline (100) silicon and a-SiC:H emitter prepared by PECVD. The photovoltaic behaviour of "raw" structures was presented in [13]. Further improvement was achieved by adding the TCO layer. This layer, as mentioned in the introduction, plays a role in an efficient collection component of photogenerated carriers which was subsequently reflected in the increase of efficiency of thus modified solar heterojunction structure.

IZO and ITO layers were prepared by RF (13.56 MHz) magnetron sputtering with varied sputtering power of 100, 140 and 180 W on SHJ solar cells and also on glass substrate. The top grid finger electrode of Al (200 nm thick) as an ohmic contact was formed using a lift off technique. The bottom side of samples was fully covered by Al ohmic contact. More details about the sample preparation were included in our previous work [13]. The targets with composition of In_2O_3-SnO_2 (In_2O_3/SnO_2 90/10 wt%) and with composition of In_2O_3-ZnO (In_2O_3/ZnO 90/10 wt%) were used for the preparation of ITO and IZO, respectively.

The solar cell sample structures were prepared on 1×1 cm^2 substrates (Fig. 1). SHJ samples were indicated in the following way: ITO-B, ITO-C and

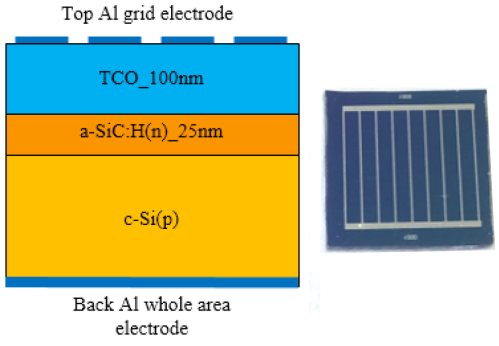

Fig. 1. Scheme and picture of SHJ sample with front TCO.

ITO-D for SHJ with ITO (IZO) layers prepared by sputtering powers 100, 140, and 180 W, respectively. The ITO-A sample was without any passivating layer. In order to characterize the prepared samples, optical and electrical measurements were performed. The transmittance was measured by Specord 2100. Electrical characterization was by the Van der Pauw and Hall method at room temperature using Ecopia HMS-5300. The DC current–voltage measurement was under AM1.5 spectrum using Keithley 2612 and AC impedance measurements were at frequencies from 100 Hz to 1 MHz using Agilent LCR 4284A.

3. Experimental results

3.1. Optical characterization and electrical resistivity

TCO layers deposited on glass underwent the Hall and optical measurements and analyses. The analysed spectra of IZO and ITO do not show any significant difference. The transmittance of both materials in the region below 400 nm is low which is related to the band gap of about 3.8 eV. The transmittance of the measured samples is over 80% in the interval from 450 to 1000 nm, indicating the maximum between 400 and 500 nm. The sample produced with the sputtering power $P_{\text{sput}} = 100$ W shows the highest value of transmittance. With the increased P_{sput} the overall transmittance decreases but toward the infrared wavelengths the transmittance is increasing again. Certainly, high transparency in visible light spectra is important to get high light generated current of solar cells with those materials on their top (Fig. 2).

The Van der Pauw and Hall measurements were carried out on samples prepared on glass to study electrical properties of TCO layers. Comparing ITO and IZO layers, lower variation of resistivity with P_{sput} is observed for IZO layers. In the case of ITO, low P_{sput} provides layers with low resistivity which increases with the increase of P_{sput}. The increase

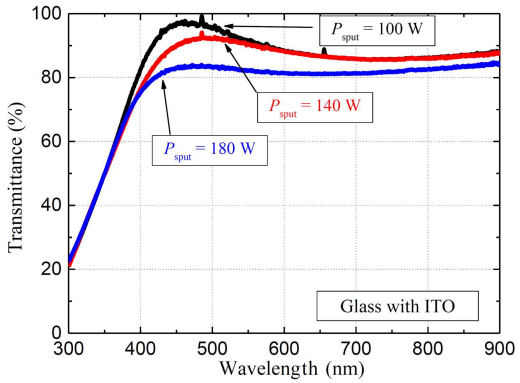

Fig. 2. Optical transmittance of ITO layers prepared with varied sputtering power P_{sput}.

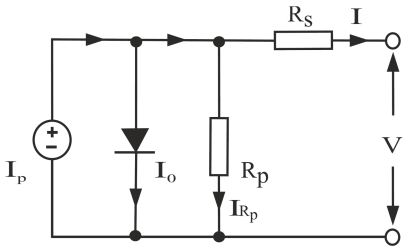

Fig. 3. Single diode model of solar cell.

of resistivity can be related to the decrease of mobility of carriers in the ITO sample. In general, the decrease of mobility is caused by the ionized impurities scattering mechanism which is the main scattering factor for structures with carrier concentration $c > 2 \times 10^{20}$ cm^{-3}. In the case of IZO, high c is observed only for the layer prepared with $P_{\text{sput}} = 100$ mA which results in the lowest mobility of 36 cm^2/(V s) for this sample. From the application point of view, the P_{sput} has a negligible influence on electrical properties of IZO. In the case of ITO, however, $P_{\text{sput}} < 140$ W is required to obtain good electrical properties of the layer [13].

3.2. DC characterization

A generally accepted model, shown in Fig. 3, of a solar cell, which properly represents its electrical behaviour, consists of a current source (light generated current I_P), a parallel diode, shunt resistance, and series resistance [14]. According to a superposition principle, the total current in the circuit is a sum of the current at dark and the current under illumination.

The output current I is in accordance with the Shockley diode equation

$$I = I_p - \frac{V+IR_s}{R_p} - I_0\left(\exp\left(\frac{V+IR_s}{nA}\right) - 1\right), \tag{1}$$

where I and V are the terminal current and voltage, I_p is the generated photocurrent, I_0 is the junction reverse current, n is the diode ideality factor and A is the so-called thermal voltage $k_{\text{B}}T/q$. Here k_{B} is the Boltzmann constant, T is the temperature and q is the elementary charge. Five parameters which characterize the treated solar cell I_{Rp}, I_0, n, R_s, and R_p are of main interest. Their values are obtainable from the measured current–voltage characteristic either in the dark or under illumination.

Currents I_0 and I_p are obtainable, e.g., using the Lambert W-function, short circuit current I_{sc}, open circuit voltage V_{oc} and the procedure described in [15]. I_0 and I_p obey (2) and (3), respectively

$$I_0 = \frac{I_{\text{sc}} + \frac{I_{\text{sc}}R_s}{R_p} - \frac{V_{\text{oc}}}{R_p}}{I_0\left(\exp\left(\frac{V_{\text{oc}}}{nA}\right) - \exp\left(\frac{I_{\text{sc}}R_s}{nA}\right)\right)}, \tag{2}$$

$$I_p = \frac{V_{\text{oc}}}{R_p} + I_0\left(\exp\left(\frac{V_{\text{oc}}}{nA}\right) - 1\right). \tag{3}$$

TABLE I

Basic parameters acquired from the I–V characteristic.

Specimen	I_{Rp} [10^{-2} A]	I_0 [10^{-6} A]	n	R_s [Ω]	R_p [10^3 Ω]
ITO-A	1.71	64.6	6.30	3.68	0.54
ITO-B	3.03	0.39	1.77	1.76	1.38
ITO-C	2.85	0.43	1.80	0.91	0.83
ITO-D	2.67	1.74	2.13	1.50	6.93
IZO-D	2.89	3.08	2.12	5.18	35.1

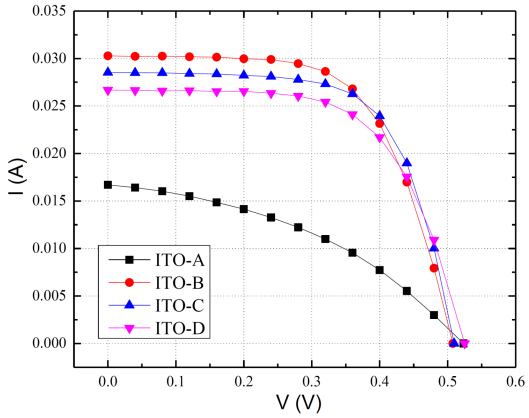

Fig. 4. I–V characteristics of ITO specimens. Points are measured values, lines are calculated values.

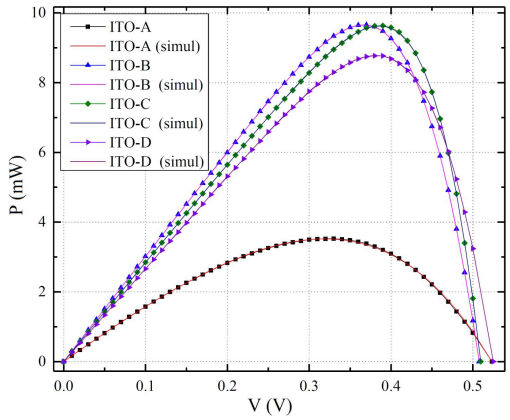

Fig. 5. Power characteristics of ITO specimens. Points are measured values, lines are calculated values.

The remaining three parameters n, R_s and R_p also result from (2) and (3). We used the Nelder–Mead type simplex search method and the least squares method as an optimization process. Finally, the generated power $P = VI$ which is going through maximum $P_{\max}$ and is equal to zero at I_{sc} and V_{oc} points. The value of fill factor FF $= P_{\max}/V_{\mathrm{oc}}I_{\mathrm{sc}}$. The obtained results at 300 K are shown in Tables I and II and in Figs. 4 and 5.

TABLE II

Output parameters of the measured specimens.

Specimen	V_{oc} [V]	I_s [10^{-2} A]	$P_{\max}$ [10^{-3} W]	FF
ITO-A	0.52	1.67	3.51	0.40
ITO-B	0.51	3.02	9.65	0.62
ITO-C	0.51	2.85	9.62	0.66
ITO-D	0.52	2.66	8.78	0.62
IZO-D	0.49	2.89	6.69	0.46

Better electrical and optical properties of ITO layers as well as contact properties with a-SiC:H suggest the ITO layer as a better choice for prepared SHJ. The best ITO sample provides efficiency up to 10% while, of course as expected, the worst behaviour is shown by the ITO-A sample being without passivation.

3.3. AC characterization

Impedance spectroscopy, in our case, was used as a complementary technique to DC analyses in order to obtain a more complex view on electrical transport processes in the structure. The effect of the reactor power during the deposition of the TCO layer can be easily recognized looking at the obtained impedance spectra. The subsequently calculated dynamic parameters such as series and parallel resistances, the constant phase element (CPE) coefficient, optical and Hall measurements and the resulting photovoltaic properties obtained from DC analyses give accurate feedback to optimize technology (in our case, the reactor power).

In order to evaluate the obtained impedance data, a numerical simulation was used to find the best fit and suitable AC equivalent circuit for the prepared structures.

The components of the AC circuit in Fig. 6 have a direct relationship to the electrical transport processes in the prepared heterostructure and are related to the used technology. Resistance R_1, which in the measured impedance diagram (Figs. 7 and 8) is represented by the distance of the semicircle from the origin of the coordinate system, is series resistance of the heterostructure.

Series resistance should be as low as possible. The parallel combination of R_2 and C_1 is linked to the space charge region of the p–n heterojunction. The combination of resistance R_3 (recombination resistance) and constant phase element (CPE) P_1 should be associated with traps and defects in the structure [16–18]. The parameter P_1, obtained using numerical simulations, means in our case the component of the AC equivalent circuit of solar cell heterojunction structure.

Electrical impedance of CPE can be expressed as

$$Z_{P_1} = Y_0^{-1}(\mathrm{i}\omega)^{-m}. \tag{4}$$

The measured impedance spectra for selected forward, reverse and zero bias for two samples, ITO-A

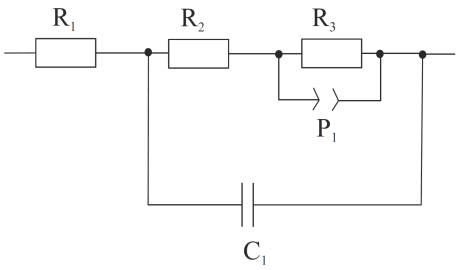

Fig. 6. Proposed AC equivalent circuit.

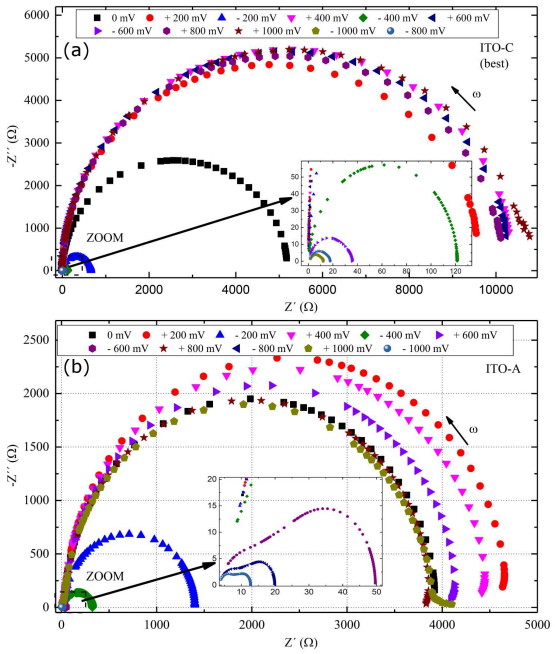

Fig. 7. AC impedance plots measured in the dark for prepared ITO-A, ITO-C solar heterostructures.

and ITO-C, are shown in Fig. 7. The advantage of impedance spectroscopy is that one can immediately recognize some aspect of the behaviour without any detailed numerical analyses.

The differences between the selected samples, and hence the effect of reactor power, are already visible on the measured data diagrams at different biases (Fig. 7). The diameter of the impedance semicircle is larger for the ITO-C sample, which was based on DC analyses (efficiency, FF and series resistance), evaluated as the best one. The diameter of the semicircle represents the shunt resistance of the structure which is infinite in an ideal case. The measured data for higher bias in the forward direction give information about the existence of structural defects (amorphous layer) and interface quality. The existence of two circles is obvious for the ITO-A sample at forward bias. For better illustration, we present in Fig. 8 impedance diagrams for all samples and selected DC biases. When comparing them, one can assume that surface states of the un-passivated ITO-A sample result in an additional relaxation process.

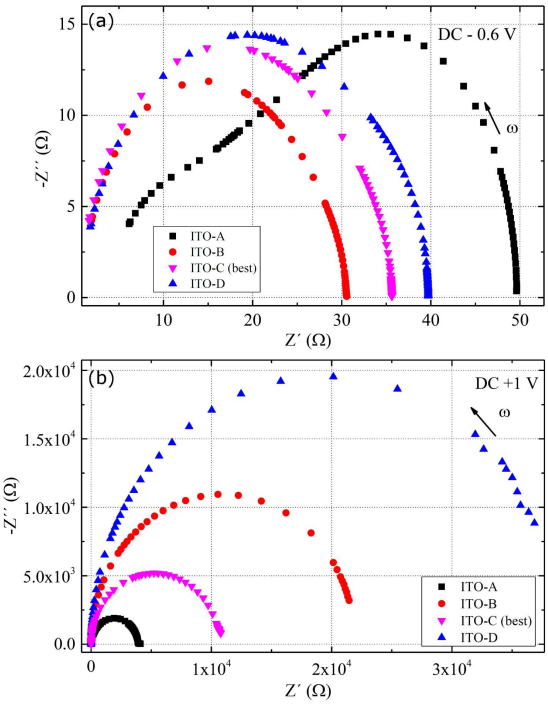

Fig. 8. AC impedance plots at forward (a) and reverse (b) DC bias measured in the dark for prepared solar heterostructures, where the sputtering power in the reactor was a parameter.

The positive influence of the passivation layer on the top surface is clearly recognizable from the diagrams in Fig. 8a. The series resistance (distance from the origin of the coordinate system) is lower when the surface was passivated by ITO (IZO). The application of the ITO layer had an impact on the reduction of series resistance as well as the reduction of the structural defects due to the passivation of unsaturated bonds on the surface. The measured impedance spectra under reverse bias (Fig. 8b) show that the change in the sputtering power results in a significant change of the value of the parallel/shunt resistance (diameter of the impedance semicircle) of prepared heterostructures.

For a more detailed assessment, fitted values of circuit elements of AC equivalent circuit for selected DC biases measured under dark conditions at 300 K are listed in Table III.

We can conclude the following outcomes:

- The voltage-dependent capacity C_1 obtained close to 0 V and toward reverse biases represents the capacity of the space charge region. The more convenient technology is reflected in the higher value of the transition capacity at low positive and reverse biases.
- Impedance measurements confirm the results obtained by DC analyses and show that the ITO-A sample has the largest series resistance (without antireflective ITO layer) 8.25 Ω at 0 V DC bias and 5.61 Ω at −0.5 V DC bias.

TABLE III

Basic parameters obtained from fitted measured impedance data.

Sample	DC bias [V]	C_1 [F]	R_1 [Ω]	R_2 [Ω]	R_3 [Ω]	P_1 [F s^{m-1}]	m
ITO-A	0	9.54×10^{-9}	8.25	126.67	3824.8	1.00×10^{-8}	0.97
	−0.5	1.86×10^{-8}	5.61	24.6	88.343	1.05×10^{-6}	0.81
ITO-B	0	1.65×10^{-8}	0.66	1534.3	2284	9.24×10^{-10}	1
	-0.5	2.86×10^{-8}	0.98	40.9	8.1749	2.38×10^{-6}	0.86
ITO-C	0	1.67×10^{-8}	0.4	1496.5	3691.5	1.52×10^{-9}	1
	−0.5	2.86×10^{-8}	0.76	50.3	10.733	1.55×10^{-6}	0.88
ITO-D	0	1.48×10^{-8}	0.33	1751	1069	1.51×10^{-9}	1
	−0.5	2.84×10^{-8}	0.92	47.4	19.266	1.47×10^{-6}	0.83

- Parallel/shunt resistance R_2 which reflects the quality of technology and represents various types of structural disorders, such as dislocations, vacancies and conductive leads, varies from 126.67 Ω for the ITO-A sample (without ITO layer) to 1751 Ω for ITO-D. A higher shunt resistance value means a better design and technology of that solar cell structure.
- Although the shunt resistance of the ITO-D sample is the highest (Fig. 7b), the value of series resistance is more critical and thus the best PV parameters were obtained on the ITO-C sample.
- Another useful feedback parameter for the technology assessment is exponent m of CPE impedance (4) which represents the character of the distribution of relaxation times — a pure capacitor when $m = 1$. The decrease of m can be explained by the production of additional structural defects such as traps, broken chemical bonds, and the related recombination centres. They are shunting the mentioned capacitor. The lowest values of m, in our case, were calculated for the sample where the TCO layer was not applied.

Spectra and data obtained from AC analyses of the sample with IZO layer are not presented here since DC parameters (and finally AC measurements and analyses) showed the use of the IZO layer in such deposition conditions adjustment not to be beneficial for the improvement of photovoltaic properties.

4. Conclusion

The experimental results were obtained on SHJ photovoltaic cell structures where there was a heterojunction between crystalline silicon and amorphous silicon carbide and the structures were passivated using the ITO/IZO layer. The optimization of preparation of those TCO layers was mainly of interest. We have shown that the deposition of TCO, in our case ITO and IZO, need to be tuned to get optimal required optical and electrical properties of consecutive produced solar cell samples. The deposition process was at sputtering power between 100 and 180 W. While the IZO layer should to be deposited at 140 W to get optimal properties, the ITO layer has shown better behaviour when the layer was deposited at lower power 100 W. The efficiency of the best prepared SHJ solar cell sample was 9.7%.

Optimization of TCO layers results in the increase of the efficiency from 3.5% for the reference sample without TCO to 6.7% and 9.7%, for IZO and ITO layers, respectively (represented by the sample with the best obtained values). A further increase of the efficiency can be achieved by: (i) applying the concept of a back surface field or (ii) applying a-Si:H(p) at the bottom of the silicon substrate to decrease a back surface recombination, (iii) inserting an a-Si:H(i) layer at the a-SiC:H/c-Si interface to decrease recombination at this interface, (iv) optimizing the front contact geometry to decrease shading effects and increase light trapping in the structure, (v) using a c-Si substrate with lower resistance and higher carrier lifetime texturisation on a c-Si substrate and by decreasing a-SiC:H thickness.

Acknowledgments

This work was supported by the Slovak Research and Development Agency under the Contract No. APVV-19-0049, APVV-17-0169 and Operational Program Integrated Infrastructure for the project: the International Center of Excellence for Research on Intelligent and Secure Information and Communication Technologies and Systems — 2nd stage, ITMS code: 313021W404, co-financed by the European Regional Development Fund.

The research was also supported by the National Research and Development Project Grant VEGA 1/0529/20.

References

[1] Z. Er, I.B. Turna, *Acta Phys. Pol. A* **129**, 865 (2016).

[2] M.A. Green, E.D Dunlop, J. Hohl-Ebinger, M. Yoshita, N. Kopidakis, Xiaojing Hao, *Progr. Photovolt.* **28**, 629 (2020).

[3] D.W. Kang, P. Sichanugrist, M. Konagai, *Electron. Mater. Lett.* **12**, 451 (2016).

[4] C. Yu, M. Yang, G. Dong et al., *Jpn. J. Appl. Phys.* **57**, 08RB15 (2018).

[5] D. Rached, H. Madani Yssad, *Acta Phys. Pol. A* **127**, 767 (2015).

[6] T. Kinoshita, D. Fujishima, A. Yano et al., in: *Proc. 26th Europ. Photovoltaic Solar Energy Conf. and Exhibition*, 2011, p. 871.

[7] K. Yoshikawa, W. Yoshida, T. Irie et al., *Sol. Energy Mater. Sol. Cells* **173**, 37 (2017).

[8] A. Valla, P. Carroy, F. Ozanne, D. Muñoz, *Sol. Energy Mater. Sol. Cells* **157**, 874 (2016).

[9] M.F. Al-Kuhaili, *J. Mater. Sci. Mater. Electron.* **31**, 2729 (2020).

[10] P.P. Manik, R.K. Mishra, U. Ganguly, S. Lodha, in: *Proc. 72nd Device Research Conference — Conference Digest, Santa Barbara (CA, USA)*, 2014.

[11] A. Way, J. Luke, A.D. Evans, Z. Li, J.-S. Kim, J.R. Durrant, H.K.H. Lee, W.C. Tsoi, *AIP Adv.* **9**, 085220 (2019).

[12] Y. Warasawa, M. Matsumoto, A. Kaijo, M. Sugiyama, in: *Proc. 2011 37th IEEE Photovoltaic Specialists Conf.*, 2011, p. 002768.

[13] M. Perný, V. Šály, V. Ďurman, M. Mikolášek, F. Janíček, J. Huran, in: *Proc. 2019 20th Int. Sci. Conf. on Electric Power Engineering (EPE)*, 2019, art. no. 8778044.

[14] G. Kanimozhi, H. Kumar, *Appl. Soft Comput.* **71**, 141 (2018).

[15] A. Jain, A. Kapoor, *Sol. En. Mater. Sol. Cells* **81**, 269 (2004).

[16] A.J. Leenheer, J.D. Perkins, M.F.A.M. van Hest, J.J. Berry, R.P. O'Hayre, D.S. Ginley, Phys. Rev. B **7**, 115215 (2008).

[17] B.J. Leever, C.A. Bailey, T.J. Marks, M.C. Hersam, M.F. Durstock, *Adv. Energy Mater.* **2**, 120 (2012).

[18] H.Y. Seba, *Thin Solid Films* **699**, 137891 (2020).